ATMOSPHERIC SCIENCE

# A previously unrecognized source of the $O_2$ Atmospheric band emission in Earth's nightglow

**Konstantinos S. Kalogerakis**



**Earth's night sky continuously produces a faint chemiluminescence known as nightglow. Two prominent nighttime emissions around 90 km are the $O_2$ Atmospheric and the OH Meinel band systems. Despite a plethora of studies since their identification seven decades ago, substantial gaps persist in our understanding of the mechanisms that control them. This report shows that oxygen atoms connect these two emissions: Fast, multiquantum, vibrational-to-electronic relaxation of OH(v) by O atoms activates a pathway that generates $O_2$ Atmospheric band emission. This newly discovered source exhibits a strong altitude dependence and can contribute a majority of the observed $O_2$ Atmospheric band emission when the peaks of the OH and O-atom layers overlap. The new findings call for a reinterpretation of Earth's nightglow emissions and a revision of relevant atmospheric models.**

## INTRODUCTION

Bright auroral displays have inspired awe for millennia. In contrast, the weak background radiation of Earth's night sky has remained relatively unnoticed (*1*, *2*). Photometric observations in the early 1900s established that starlight and scattered light combined could not account for the brightness of the sky and provided the first quantitative information on the variability of nighttime spectral features (*3*, *4*). This knowledge planted a fertile seed for the field of upper atmospheric science known as aeronomy, and numerous studies of the nightglow ensued. Initially, emphasis was placed on emission from atomic oxygen, but by the middle of the 20th century, excited molecular species were known to be important for the nightglow (*1*).

Photochemical processes initiated by solar radiation in the upper atmosphere during the day yield energetic atoms and molecules, some of which emit radiation—referred to as dayglow and nightglow depending on when the emission occurs. The $O_2$ Atmospheric and OH Meinel band emissions (Fig. 1A) are two important nightglow features (*1*). Resolved spectra of both emissions were first recorded from ground-based observations by astronomer Aden B. Meinel in 1948 (*5*). The identification of the (0,1) $O_2(b^1\Sigma_g^+ - X\,^3\Sigma_g^-)$ Atmospheric band (AB) emission near 864.5 nm was enabled by its detection in laboratory discharge afterglows a year earlier (*6*). In contrast, no laboratory comparison was available for the OH Meinel band emission in 1948, and its identity was confirmed 2 years later (*7*–*10*).

Reliable interpretation of nightglow requires understanding how the emitting layer comes to existence. Therefore, detailed knowledge of the relevant photochemical production mechanisms is needed. The processes that consume the emitting species are just as important, and the observed intensity reflects the competition of the production and loss pathways.

The source of vibrationally excited OH in the upper atmosphere is the highly exothermic reaction of hydrogen atoms with ozone (*1*, *7*, *8*, *11*, *12*)

$$H + O_3 \rightarrow OH(v = 5\text{–}9) + O_2 \quad (1)$$

Water photodissociation gives rise to a layer of hydrogen atoms, whereas the three-body association O + $O_2$ + M (M = $N_2$, $O_2$) is responsible for the generation of ozone (*1*, *7*, *8*). The OH Meinel band emission involves transitions between rotational-vibrational levels within the OH ground state (Fig. 1B). The emission varies as a function of geographic location, time, and season. Its altitude profile exhibits a peak near 87 km with a full-width-at-half-maximum value of approximately 8 km (*13*). Most of the available energy from the H + $O_3$ reaction is released into the OH product. The highest energetically allowed vibrational level, $v = 9$, is also the most probable nascent level (*11*, *12*). Nevertheless, collisional relaxation efficiently redistributes the initial OH($v$) excitation, and the observed emission indicates a steady-state vibrational population distribution that markedly differs from the nascent one, i.e., generated by the H + $O_3$ reaction in the absence of collisions (Fig. 1C) (*12*, *14*).

The maximum intensity of the $O_2$ AB emission usually occurs near 94 km, a few kilometers below the maximum of the O-atom concentration (*15*–*18*). Three-body O-atom association, O + O + M (M = $N_2$, $O_2$), to form molecular oxygen is considered the source of this emission at night. This process generates all the low-lying electronic states of $O_2$ (Fig. 1D). The nascent $O_2$ molecule is initially formed near the dissociation limit, and the shallow $^5\Pi_g$ electronic state at large internuclear distance is believed to play an important "gateway" role (*15*, *16*). Collision-induced vibrational relaxation, electronic energy exchange, and intersystem crossings redistribute the nascent molecules among the low-lying $O_2$ electronic states and eventually populate the emitting $O_2(b^1\Sigma_g^+)$ state. The $O_2(b^1\Sigma_g^+, v = 0)$ vibrational level generates the strongest emission because it is chemically inert (*15*, *16*). The most intense emission band, (0,0) $O_2(b^1\Sigma_g^+ - X\,^3\Sigma_g^-)$ near 762 nm, is approximately 21 times stronger than the (0,1) band near 864.5 nm but can only be observed from space because it is absorbed by Earth's atmosphere (*16*). Nightglow emission from higher $O_2(b)$ vibrational levels has also been observed, but it is extremely weak (*16*). Any subsequent mention of the $O_2$ AB will refer to emission from the (0,0) band.

Since the 1980s (*15*–*18*), the generally accepted mechanism for the generation of $O_2$ AB emission has been

$$O + O + M \rightarrow O_2^* + M\ (M = O_2, N_2) \quad (2)$$

$$O_2^* + O_2 \rightarrow O_2(b, v = 0) + O_2 \quad (3)$$

$$O_2(b, v = 0) \rightarrow O_2(X) + h\nu \quad (4)$$

Center for Geospace Studies, SRI International, Menlo Park, CA, USA. Email: ksk@sri.com

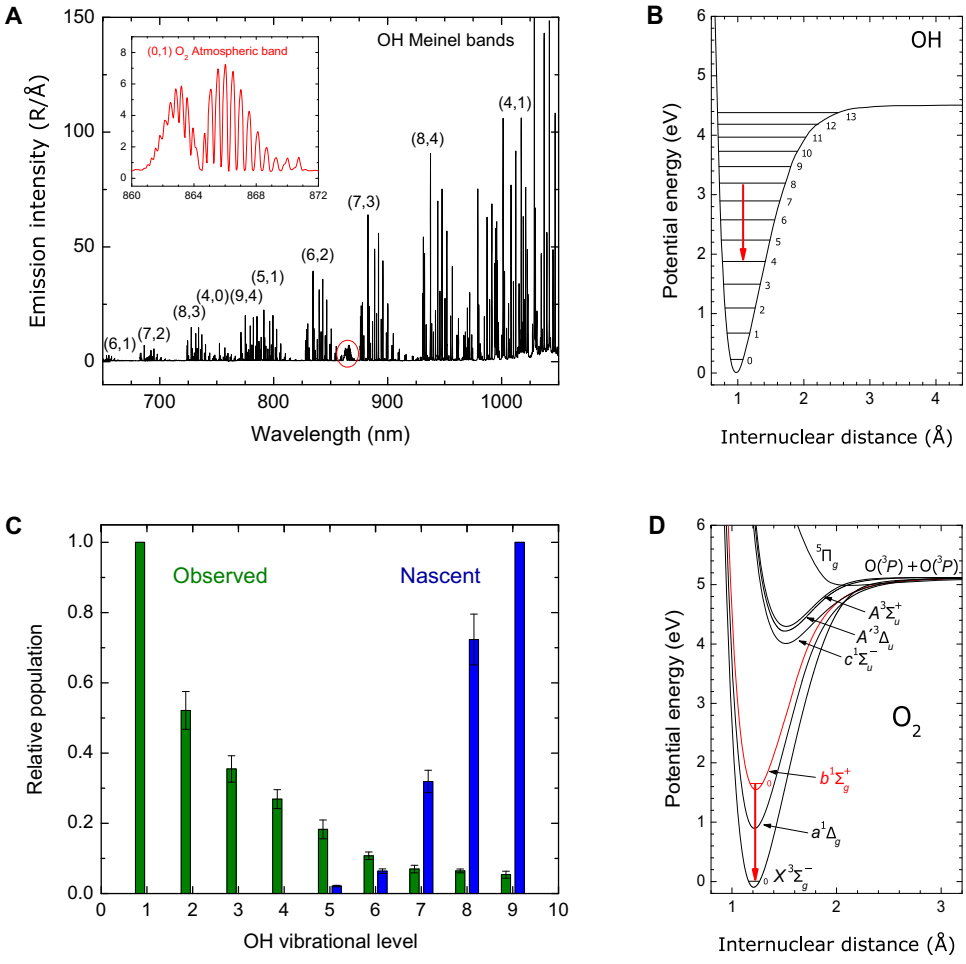


**Fig. 1. The OH Meinel and $O_2$ AB systems are important features of the nightglow.** (**A**) Astronomical night sky spectrum obtained using the Echelle Spectrograph and Imager on the Keck II telescope displays strong OH Meinel band emission (4 March 2000, 8:58 UT; λ/Δλ, ~7000; 50-min exposure) (*14*). The inset shows the weak (0,1) band of the $O_2$ AB system near 864.5 nm. (**B**) Potential energy curve and vibrational levels of the OH ground state. The red arrow indicates a representative OH Meinel feature—the (8,4) band near 937 nm. (**C**) Observed OH vibrational population distribution in the nightglow (green) and nascent distribution from the H + $O_3$ reaction (blue) (*12*, *14*). (**D**) Low-lying electronic states of $O_2$. The red arrow indicates the strong (0,0) $O_2$ ($b^1\Sigma_g^+ - X^3\Sigma_g^-$) emission near 762 nm that is absorbed by the atmosphere and is observable only from space.

where $O_2$* is an electronically excited precursor that leads to the emitting level following collisions with ground-state $O_2$ molecules and $h\nu$ represents the emitted photon.

Despite numerous investigations of these two nightglow emissions during the past seven decades, notable gaps persist in our knowledge. Regarding the OH Meinel band emission, the applicable relaxation processes and observed rotational and vibrational population distributions are only partially understood. For the $O_2$ AB emission, the details of its production mechanism, the relevant intermediate precursors, and their yields remain elusive. The empirical equations used in the literature to relate its intensity to the O-atom concentration generally account for the observed emission and altitude dependence (*17*, *18*), but the underlying processes and scaling factors used have not been confirmed by laboratory experiments. Moreover, as shown in reactions 2 to 4, these processes consider only collisions of $O_2$ with the precursor excited state. Laboratory experiments determined comparable rate constants for vibrational relaxation of $O_2(b, v = 1)$ by O and $O_2$ and thus cast doubt on the validity of the assumption that O atoms have no role in the excitation transfer step of reaction 3 (*19*, *20*). The aforementioned problems have stubbornly persisted for decades because these nightglow emissions depend on interactions involving atmospheric species such as atomic hydrogen and oxygen that are extremely difficult to probe in situ and in the laboratory.

## RESULTS

### Laboratory studies reveal a previously unrecognized source of nighttime O($^1D$) atoms and $O_2$ AB emission

Approximately a decade ago, experiments investigating OH collisional relaxation yielded an unexpected result: The deactivation of OH($v = 9$) by ground-state O($^3P$) atoms was found to be extremely fast, with a total removal rate constant of $(4 \pm 1) \times 10^{-10}$ cm$^3$ s$^{-1}$ at room temperature (*21*). Such a large value approaches the gas-kinetic limit and, at first, could not be accommodated in atmospheric models (*22*–*24*). This quandary defied a solution until recently (*25*, *26*), when laboratory measurements demonstrated that the interaction of OH($v$) with O atoms

involves a fast, spin-allowed, multiquantum, vibrational-to-electronic (V-E) energy transfer pathway that generates excited $O(^1D)$

$$OH(v \geq 5) + O(^3P) \rightarrow OH(0 \leq v' \leq v - 5) + O(^1D) \quad (5)$$

An example of this process for $OH(v = 9)$, the major nascent product of $H + O_3$, is

$$OH(v = 9) + O(^3P) \rightarrow OH(v = 3) + O(^1D) \quad (6)$$

Multiquantum V-E relaxation by O atoms was found to be the most efficient loss process for $OH(v = 9)$ and provided an explanation for the unexpectedly large total removal rate constant (*25*).

During the day, $O(^1D)$ is generated from photodissociation of $O_2$ and $O_3$ by solar radiation at altitudes near 90 km. These processes do not occur at night, but the OH(high $v$) + O multiquantum relaxation provides a source of nighttime $O(^1D)$ atoms. This source was recently shown to result in enhanced $CO_2$ 4.3-μm emission via energy transfer from $O(^1D)$ to $N_2$ and then to $CO_2$ and thus explained unacceptably large discrepancies between observations and model calculations of the nighttime $CO_2$ 4.3-μm emission that persisted for several decades (*27*).

The $O(^1D)$ atoms generated by the OH(high $v$) + O multiquantum vibrational relaxation process also provide a significant source of $O_2$ AB emission. $O(^1D)$ atoms rapidly transfer energy to ground-state $O_2$ and generate electronically excited $O_2(b)$ molecules (*28*, *29*)

$$O(^1D) + O_2 \rightarrow O_2(b, v = 0, 1) + O(^3P) \quad (7)$$

This process is important in the dayglow (*29*) but has never been considered for the nighttime $O_2$ AB emission. The availability of $O(^1D)$ from the multiquantum relaxation process of reaction 5 leads to the efficient production of $O_2(b, v = 0)$ because collisions with $O_2$ rapidly relax $O_2(b, v = 1)$ to $O_2(b, v = 0)$ (*20*). From the atmospheric composition and the rate constants for $O(^1D)$ relaxation by $N_2$ and $O_2$, we can estimate that $O_2$ deactivates approximately 25% of $O(^1D)$ for altitudes near the OH layer (*30*, *31*). As a result, the OH layer provides a source of the $O_2$ AB emission, and O atoms represent the link that connects these two nightglow emissions.

## Estimates of the OH($v$) + O source and observations with sounding rockets

The sounding rocket campaigns Energy Transfer in the Oxygen Nightglow (ETON; multiple rockets launched on 23 March 1982 from South Uist, Scotland) and Non-local Thermodynamic Equilibrium (NLTE; two rockets launched in March 1998 from Esrange, Sweden) measured the $O_2$ AB emission and O atoms under geomagnetically quiet conditions (*17*, *32*). Here, we present an analysis of these observations that demonstrates the importance of the new $O_2$ AB emission source. Only $OH(v = 9)$ is considered because this is the only vibrational level for which the relevant kinetics parameters have been confirmed in laboratory measurements. Additional contributions to the $O_2$ AB emission can be expected to the extent that process 5 is active for $OH(v = 5$ to $8)$. A compelling indication that this may be the case arises from the success of recent efforts to model the OH Meinel band and $CO_2$ 4.3-μm emissions (*27*) and to retrieve O atoms from OH Meinel band observations (*33*). These calculations determined that considering $OH(v = 5$ to $8)$

**Table 1. Processes and relevant kinetics parameters used in the calculation of the contributions of OH($v$ = 9) + O multiquantum vibrational relaxation to the $O_2$ AB emission.** When a kinetics data compilation is available, that reference is shown for the sake of brevity. Additional details are provided in Methods.

| Process | Parameter | Value | | *f*, *g** | Reference |
|---|---|---|---|---|---|
| | | 298 K (±%) | *k*(*T* Kelvin) | | |
| $H + O_3 \rightarrow OH(v) + O_2$ | $k_{HO3}$ | $2.9 \times 10^{-11}$ cm$^3$ s$^{-1}$ (±10%) | $1.4 \times 10^{-10} \times \exp(-470/T)$ | 1.1, 40 | (*31*) |
| Yield of $OH(v = 9)$ from $H + O_3$ | $y_9$ | 0.47 | | | (*12*) |
| $O + O_2 + M \rightarrow O_3 + M$ | $k_{OO2M}$ | $6 \times 10^{-34}$ cm$^6$ s$^{-1}$ (±10%) | $6 \times 10^{-34} \times (300/T)^{2.4}$ | 1.1, 50 | (*31*) |
| $O + O_3 \rightarrow O_2 + O_2$ | $k_{OO3}$ | $8 \times 10^{-15}$ cm$^3$ s$^{-1}$ (±10%) | $8 \times 10^{-12} \times \exp(-2060/T)$ | 1.1, 200 | (*31*) |
| $OH(v = 9) + O_2 \rightarrow$ products | $k_{OH9O2}$ | $2.2 \times 10^{-11}$ cm$^3$ s$^{-1}$ (±14%) | $1.15 \times 10^{-11} \times \exp(+195/T)$ | | (*21*, *25*) |
| $OH(v = 9) + N_2 \rightarrow$ products | $k_{OH9N2}$ | $7 \times 10^{-13}$ cm$^3$ s$^{-1}$ (±14%) | $5.03 \times 10^{-13} \times \exp(+100/T)$ | | (*21*, *25*) |
| $OH(v = 9) + O \rightarrow$ products | $k_{OH9O}$ | $4 \times 10^{-10}$ cm$^3$ s$^{-1}$ (±12%) | $6.2 \times 10^{-10} \times \exp(-135/T)$ | | (*21*, *25*) |
| $OH(v = 9) + O \rightarrow OH(v = 3) + O(^1D)$ | $k_{OH9NM}$ | $3.2 \times 10^{-10}$ cm$^3$ s$^{-1}$ (±16%) | $5.0 \times 10^{-10} \times \exp(-135/T)$ | | (*25*, *26*) |
| $O(^1D) + N_2 \rightarrow O(^3P) + N_2$ | $k_{ODN2}$ | $3.1 \times 10^{-11}$ cm$^3$ s$^{-1}$ (±10%) | $2.15 \times 10^{-11} \times \exp(+110/T)$ | 1.1, 20 | (*31*) |
| $O(^1D) + O_2 \rightarrow O(^3P) + O_2$ | $k_{ODO2}$ | $4.0 \times 10^{-11}$ cm$^3$ s$^{-1}$ (±10%) | $3.3 \times 10^{-11} \times \exp(+55/T)$ | 1.1, 10 | (*31*) |
| Yield of $O_2(b)$ from $O(^1D) + O_2$ | $y_{O2b}$ | 0.8 (±25%) | | | (*31*) |
| $O_2(b, v = 0) + N_2 \rightarrow O_2 + N_2$ | $k_{O2bN2}$ | $2.1 \times 10^{-15}$ (±10%) | $1.8 \times 10^{-15} \times \exp(+45/T)$ | 1.1, 100 | (*31*) |
| $O_2(b, v = 0) + O_2 \rightarrow O_2 + O_2$ | $k_{O2bO2}$ | $3.9 \times 10^{-17}$ cm$^3$ s$^{-1}$ (±50%) | | 1.5 | (*31*) |
| $O_2(b, v = 0) + O \rightarrow$ products | $k_{O2bO}$ | $0/8.0 \times 10^{-14}$ cm$^3$ s$^{-1}$ | | | (*31*) |

*The parameters $f$ and $g$ can be used to estimate the rate constant uncertainty from the expression: $(T) = (298\ K) \times \exp\{abs[g \times (1/T - 1/298)]\}$. The calculated uncertainty corresponds approximately to 1 SD (*31*).

multiquantum relaxation by O atoms together with OH($v$ = 9) + O is required to reproduce the observed OH vibrational population distribution and the magnitude of the enhancement in the $CO_2$ 4.3-μm emission. The kinetics parameters used for the OH($v$ = 5 to 8) + O processes were estimated on the basis of currently available knowledge (*27*) but have yet to be confirmed. As mentioned above, for the purpose of demonstrating the existence of the new source of the $O_2$ AB emission in this report, we restrict the calculations to the more extensively studied OH($v$ = 9) + O process. Thus, the estimates for the $O_2$ AB new source from OH($v$ = 9) + O reported here should be considered lower limits. Table 1, Methods, and the Supplementary Materials provide detailed information on the relevant mechanistic steps, equations, and chemical kinetics parameters used.

Figure 2 demonstrates that OH($v$ = 9) + O multiquantum relaxation is an important source of $O_2$ AB emission. The figure presents observations from the ETON and NLTE-2 sounding rocket campaigns together with the corresponding atomic oxygen profiles and calculations of the $O_2$ AB emission generated from the OH($v$ = 9) + O source. In each case, two estimates that reflect limiting values for the removal rate constant of $O_2(b, v = 0)$ by O atoms (see detailed discussion in Methods) are shown. A key feature of the two datasets of Fig. 2 is that they are characterized by significant differences in the measured altitude profiles for O atoms (Fig. 2B). For the ETON measurement, the O-atom layer peaks near 102 km. In contrast, during the NLTE-2 flight, downward transport of the O-atom layer appears to have shifted the number density maximum to a much lower altitude, 90 km. This altitude coincides with the region where the peak of the vibrationally excited OH layer appears and provides a key test for the OH($v$) + O source. The more extensive the overlap of the OH and O-atom layers, the stronger the $O_2$ AB emission expected from OH($v$) + O. Thus, despite the larger O-atom peak concentration measured during ETON, the lower altitude of the O-atom layer maximum and better overlap with the OH layer in the case of NLTE-2 explain the substantially stronger NLTE-2 $O_2$ AB emission compared with ETON. The results of Fig. 2 demonstrate that the new pathway originating from OH($v$ = 9) + O relaxation is an important source of $O_2$ AB emission. In the case of NLTE-2 measurements, where the O-atom and OH layers overlap optimally, the new pathway represents more than half of the observed emission.

Figure 3 compares the ETON and NLTE-2 data with the estimates of the $O_2$ AB emission from the OH($v$) + O source and possible contributions from O + O + M recombination for upper and lower limit scenarios. Additional details on these comparisons and relevant calculations are presented in Methods and the Supplementary Materials. The rocket observations and model calculations shown in Fig. 3 show overall good agreement. This is a promising result with the caveat that all the processes of interest are not fully quantified yet. Discussion and Methods consider the limitations of the current state of knowledge. A key point to highlight is that if process 5 is confirmed to be active for OH($v$ = 5 to 8) with similar rate constants to OH($v$ = 9), then the new source of $O_2$ AB emission will be the dominant source below approximately 95 km. Notably, the steady-state population in vibrational levels OH($v$ = 5 to 8) is almost one order of magnitude larger than that in OH($v$ = 9) (Fig. 1C) (*12*, *14*), which implies that even smaller rate constants for OH($v$ = 5 to 8) + O should be expected to have non-negligible contributions.

## DISCUSSION

Besides its fundamental significance for molecular energy transfer, the new OH($v$) + O multiquantum vibrational relaxation pathway of reaction 5 represents an important advancement in our understanding of nightglow emissions. These processes have several implications for the nighttime upper atmosphere that relate to the determination of its composition by remote sensing, understanding the energy flow and

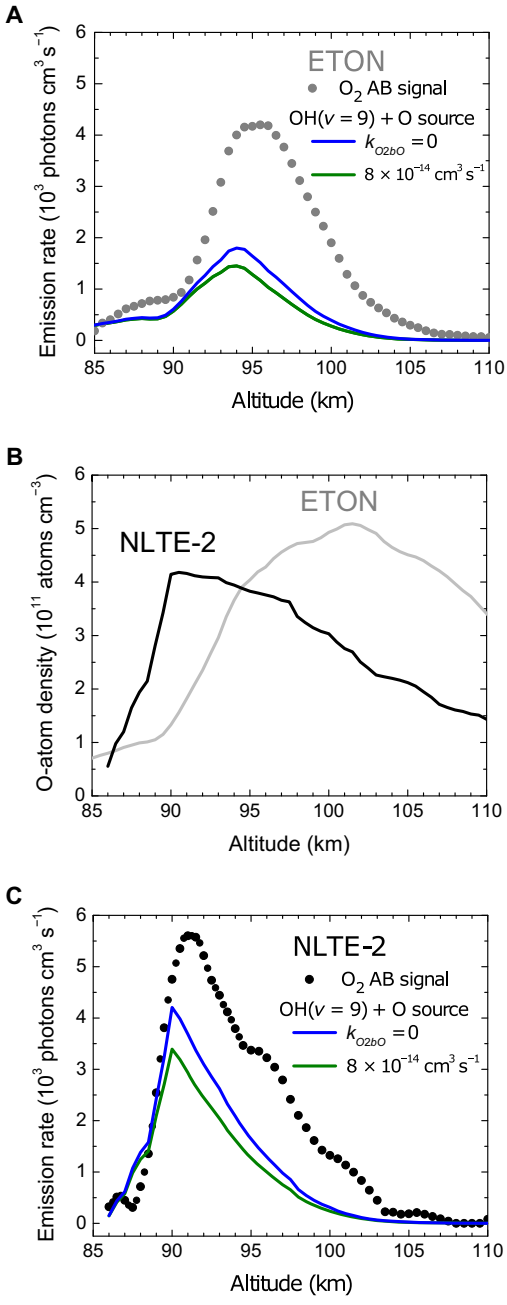


**Fig. 2. The OH($v$) + O source of $O_2$ AB emission depends on the altitude profile of the O-atom layer.** (**A** and **C**) Measured (0,0) $O_2$ AB volume emission rate as a function of altitude for ETON (gray circles) and NLTE-2 (black circles) and calculated contributions of the source from OH($v$ = 9) + O using the lower and upper limit rate constant values of 0 (blue) and 8 × 10$^{-14}$ cm$^3$ s$^{-1}$ (green) for removal of $O_2(b, v = 0)$ by O atoms. (**B**) Measured atomic oxygen number density as a function of altitude for ETON (gray) and NLTE-2 (black). Note that despite the larger O-atom density during ETON, the better overlap of the O-atom profile with the OH layer during NLTE-2 leads to stronger $O_2$ AB emission originating from OH($v$ = 9) + O.

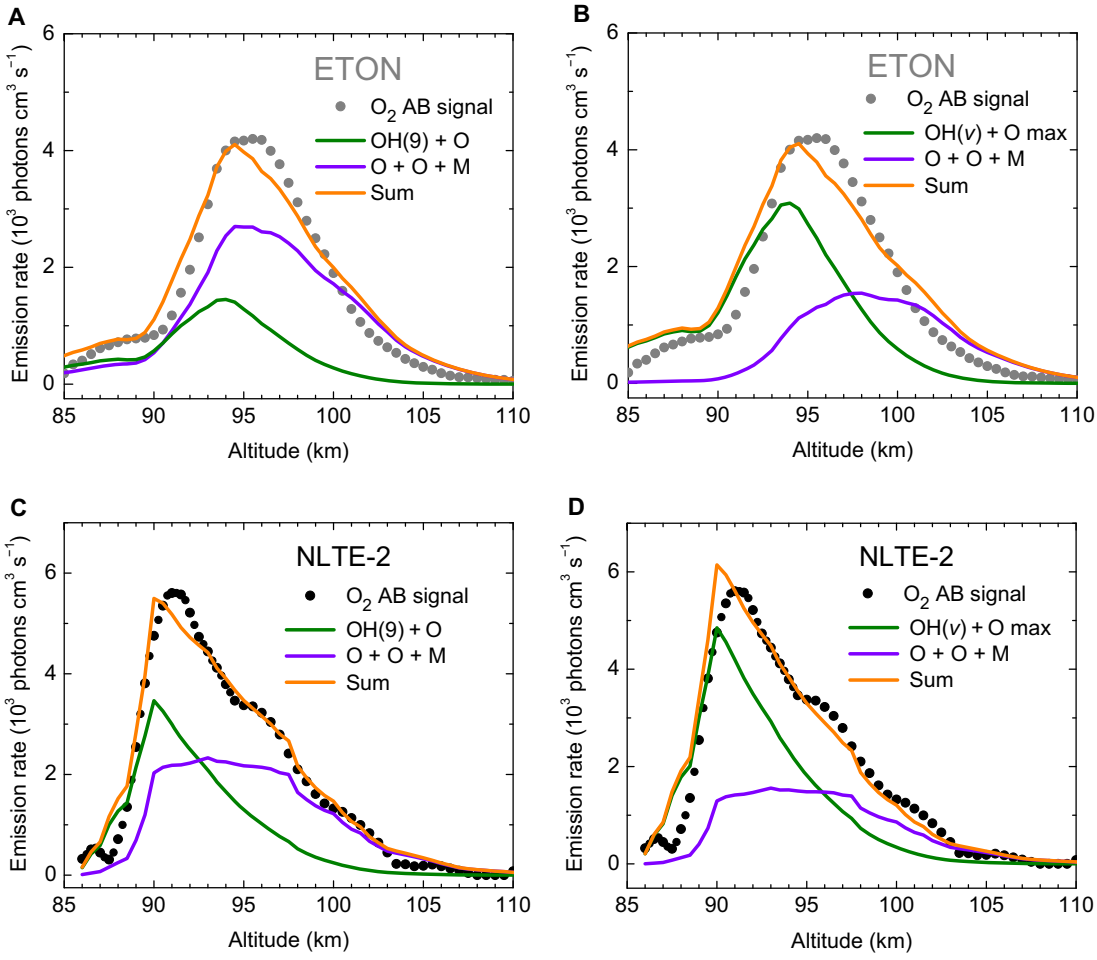


**Fig. 3. Estimated contributions from OH($v$) + O and O + O + M to the $O_2$ AB emission.** (**A** and **C**) Measured (0,0) $O_2$ AB volume emission rate profiles for the ETON and NLTE-2 datasets (gray and black circles, respectively) and calculated contributions from OH($v$ = 9) + O (green) and O + O + M (violet). The sum of the two contributions is also shown (orange) (see Methods for additional information). (**B** and **D**) As in (A) and (C) for O + O + M and assuming as an upper limit that OH($v$ = 5 to 8) produced from the H + $O_3$ reaction exhibits a behavior similar to OH($v$ = 9) + O. OH($v$) + O and O + O + M are assumed to be the only active sources of the $O_2$ AB emission.

chemical heat deposition, diurnal and seasonal variability, atmospheric circulation, wave propagation, and winds. Because the altitude region around 100 km cannot be easily studied in situ, nightglow emission signatures observed from space- and ground-based instruments are commonly used as proxies for the concentration of atmospheric species. Monitoring their intensity and temporal evolution by remote sensing provides the method of choice to study the phenomena mentioned above. These observations can be reliably interpreted only when the mechanistic details of the underlying processes are understood and quantified at the atomic and molecular level.

The H + $O_3$ and the O + O + M reactions are two of the most important sources of chemical energy release in this region of the atmosphere, often referred to as mesosphere and lower thermosphere (MLT). Most of the energy released from the newly formed chemical bonds of the above two reactions initially appears as excited OH (vibration and rotation) for the former reaction and excited $O_2$ (electronic, vibrational, and rotational) for the latter reaction. Collisional processes influence the pathways of the energy flow through the dense manifold of excited quantum levels and thus the heating efficiency, i.e., the fraction of the chemical energy that ends up as kinetic energy of atmospheric gases. Consequently, the rate and altitude dependence of chemical energy deposition is strongly influenced by the location, altitude profile, and transport dynamics of the atomic oxygen layer. A portion of the released energy is radiated into space, which, in turn, implies that detailed knowledge of the processes involved is required to quantify the energy balance of the nighttime MLT region and to fully understand the overall response of the atmosphere to the daily solar forcing, the solar cycle, other long-term changes, and transient disturbances such as geomagnetic storms.

O atoms represent key reactive species for the MLT and are intimately connected to nightglow emissions. An important point is that the number density of O atoms in the MLT region exhibits a steep gradient that guarantees a strong altitude dependence for the processes that O atoms influence, including the multiquantum vibrational relaxation pathways of reaction 5. For example, the volume mixing ratio of O atoms is approximately $5 \times 10^{-4}$ at 85 km and increases by as much as two orders of magnitude near 100 km (*17*, *30*). This altitude dependence also affects vertical tidal transport of O atoms. Because direct in situ measurements of the O-atom concentration are difficult, a detailed knowledge of nightglow emissions allows us to infer from them

the atomic oxygen concentration profile. Recent model calculations that used observations by the Sounding of the Atmosphere using Broadband Emission Radiometry (SABER) instrument on board the Thermosphere Ionosphere Mesosphere Energetics and Dynamics (TIMED) orbiter mission and included the OH($v$) + O multiquantum vibrational relaxation processes of Eq. 5 retrieved atomic oxygen concentrations 20 to 50% lower than previous analyses (*33*). The revised concentration of atomic oxygen reduced the mean chemical heating rate at an altitude near 90 km by 10 K/day and the mean radiative cooling by $CO_2$ emission at 15 μm by 2 K/day, thus bringing the global annual chemical heating and radiative cooling rates near balance (*33*).

The OH($v$) + O source of the $O_2$ AB emission signifies that $O_2$ electronically excited states are not generated only by the O + O + M association process, as previously thought. The emission resulting from the OH($v$) + O source favors the lower altitude range in which the nighttime $O_2$ AB emission is observed (Fig. 2, A and C). Assuming that no other source for $O_2$ AB exists, the difference between the observed $O_2$ AB and the OH($v$) + O source can be attributed to O-atom association. Therefore, the mechanism adopted during the past four decades for $O_2$ AB generation by O + O + M does not adequately describe the altitude dependence of the difference. Additional details and suggestions for improvements based on what we know from recent laboratory studies are provided in Methods. Looking forward, it is crucial to determine the role of the multiquantum vibrational relaxation pathways OH($v$ = 5 to 8) + O, so that together with OH($v$ = 9) + O, we can fully quantify the OH($v$) + O source of the nighttime $O_2$ AB emission. This is also a key first step for future efforts to better understand the mechanistic details of O-atom association and the cascade pathways through the quantum-state manifold of electronically excited $O_2$.

## CONCLUSION

O atoms have an even more complex and elaborate role in the upper atmosphere than previously appreciated. Their interaction with OH($v$) leads to $O_2$ AB emission, and thus, O atoms effectively connect the two emissions. The new findings call for a reinterpretation of Earth's nightglow emissions and a revision of relevant atmospheric models. This report opens a new chapter for Earth's upper atmospheric nightglow emissions and aims to stimulate synergistic efforts between observers, modelers, theoreticians, and experimentalists to further deepen our understanding of planetary atmospheres.

## METHODS

This section begins with a presentation of the formulas used to estimate the new source of $O_2$ AB emission. Next, we provide information on the datasets and model atmosphere inputs used for the calculations. We then discuss the parameters of Table 1 and relevant uncertainties and elaborate on the results by providing additional comments and a consistency check. Last, the focus shifts to the O + O + M association reaction and the implications for this process with regard to the $O_2$ AB emission.

### Calculation of $O_2$ AB emission from OH($v$ = 9) + O

The steps that control the generation of $O_2$ AB emission from OH($v$ = 9) + O collisions can be summarized in reactions M1 to M9. Process M4, loss by atmospheric species, includes inelastic scattering and reaction with O atoms that leads to $O_2$ and hydrogen atoms (*31*). Process M5 is the key step that generates $O(^1D)$ and effectively couples the OH Meinel and the $O_2$ AB emissions. Loss of $O(^1D)$ by ground-state O atoms is negligible for the altitude range considered here (*34*)

$$O + O_2 + M \rightarrow O_3 + M\ (M = O_2, N_2, O) \quad \text{(M1)}$$

$$H + O_3 \rightarrow OH(v = 9) + O_2 \quad \text{(M2)}$$

$$O_3 + O \rightarrow O_2 + O_2 \quad \text{(M3)}$$

$$OH(v = 9) + M \rightarrow \text{products}(M = O_2, N_2, O) \quad \text{(M4)}$$

$$OH(v = 9) + O(^3P) \rightarrow OH(v = 3) + O(^1D) \quad \text{(M5)}$$

$$O(^1D) + N_2 \rightarrow O(^3P) + N_2 \quad \text{(M6)}$$

$$O(^1D) + O_2 \rightarrow O_2(b, v = 0, 1) + O(^3P) \quad \text{(M7)}$$

$$O_2(b, v = 1) + O_2 \rightarrow O_2(b, v = 0) + O_2 \quad \text{(M8)}$$

$$O_2(b, v = 1) + O \rightarrow O_2(b, v = 0) + O \quad \text{(M9)}$$

We applied the steady-state approximation to chemical species $O(^1D)$, OH($v$ = 9), and $O_3$. The assumption of photochemical equilibrium in the mesosphere is often used in the literature (*12*, *35*–*37*). It is a reasonable approximation for this case that concerns rapid, local measurements of slowly varying nightglow emissions. The steady-state concentration of OH($v$ = 9) and $O_2$($b$, $v$ = 0) generated from source (M5) is described by the equations

$$[OH_9] = y_9 \times k_{OO2M} \times k_{HO3} \times [O] \times [O_2] \times [M] \times [H] / \{LT(OH_9) \times LT(O_3)\} \quad \text{(M10)}$$

$$[O_{2b0}] = [OH_9] \times y_{O2b} \times k_{OH9NM} \times k_{ODO2} \times [O] \times [O_2] / \{LT(O^1D) \times LT(O_{2b0})\} \quad \text{(M11)}$$

where $[M] = [O_2] + [N_2] + [O]$. The yields $y_i$ and rate constants $k_i$ are listed in Table 1. The factors LT represent the loss terms for OH($v$ = 9), $O_2$($b$, $v$ = 0), $O_3$, and $O(^1D)$, respectively

$$LT(OH_9) = A_9 + k_{OH9O} \times [O] + k_{OH9O2} \times [O_2] + k_{OH9N2} \times [N_2] \quad \text{(M12)}$$

$$LT(O_{2b0}) = A_{O2b} + k_{O2bO} \times [O] + k_{O2bO2} \times [O_2] + k_{O2bN2} \times [N_2] \quad \text{(M13)}$$

$$LT(O^1D) = A_{OD} + k_{ODO2} \times [O_2] + k_{ODN2} \times [N_2] \quad \text{(M14)}$$

$$\mathrm{LT}(O_3) = k_{HO3} \times [H] + k_{OO3} \times [O] \quad \text{(M15)}$$

A$i$ are the relevant radiative decay rates for O($^1D$), the (0-0) band of the $O_2$ AB emission, the total emission from $O_2(b, v = 0)$, and OH($v = 9$), with values 0.009, 0.079, 0.083, and 173 $s^{-1}$, respectively (*31*, *38*, *39*). The observed volume emission rate for an atmospheric species at the altitude of interest is given by the product of its radiative decay rate and number density.

## Data and model atmosphere

The ETON campaign was launched on 23 March 1982 from the island of South Uist in Scotland (57.36°N, 7.38°W). Multiple rockets measured atomic and molecular nightglow emissions as well as the atomic oxygen density profile (*17*, *40*). ETON payloads P230H and P227H, from which the observed $O_2$ AB emission profiles were used here, were launched at 21:27:17 UT and 22:10:51 UT, respectively (*17*).

The NLTE campaign comprised two rockets launched from the Esrange Space Center (68°N, 21°E), Sweden in March 1998 (*32*, *41*). The payload of the second rocket, NLTE-2, was launched on March 6 at 21:26:00 UT and included photometric measurements of the $O_2$ AB emission with simultaneous monitoring of atomic oxygen.

The atmospheric composition, [$N_2$], [$O_2$], [H], and temperature inputs were taken from the NRLMSISE-00 model (*30*) for the time and date of each dataset. For the atomic oxygen profile, we used the observations of ETON payload P232H and NLTE-2 descent flight. In our discussion of possible sources of error, we will revisit the atomic oxygen profiles used.

## Parameter inputs and relevant uncertainties

Table 1 lists information on the input parameters used to calculate the contributions of the OH($v = 9$) + O multiquantum relaxation to the $O_2$ AB emission. The table shows the values and associated uncertainty estimates at 298 K and, where available, an expression that describes their temperature dependence. The latest Evaluation on Chemical Kinetics of the Jet Propulsion Laboratory (JPL) was the reference of choice for several processes (*31*). Additional comments are provided next.

For the rate constant of the H + $O_3$ reaction, experimental studies by Liu *et al.* (*42*) have corroborated the most recent JPL recommendation and provided new measurements at low temperatures. The yield of OH($v = 9$) from H + $O_3$ used in this work follows the recommendation of Adler-Golden (*12*), which was based on the critical evaluation by Steinfeld *et al.* (*43*). The OH($v = 9$) total removal rate constant for collisions with O, $O_2$, and $N_2$ as well as the rate constant for the OH($v = 9$) + O multiquantum relaxation adopted the values reported by Kalogerakis *et al.* and Sharma *et al.* (*21*, *25*, *26*) and assumed a temperature dependence similar to that observed by Thiebaud *et al.* (*44*). For the collisional relaxation of $O_2(b, v = 0)$ by $O_2$, $N_2$, and O, the values of the current JPL evaluation were used (*31*). Because of the uncertainty in the rate constant for $O_2(b, v = 0)$ by O, measured by Slanger and Black (*45*) at 298 K, and the lack of studies at low temperatures, a common practice in the literature (*17*, *18*, *32*) has been to use a lower limit of zero and a high value of $8 \times 10^{-14}$ $cm^3$ $s^{-1}$, i.e., the measured rate constant at room temperature. We adopted this approach and, in Fig. 2, show results for the new source of $O_2$ AB from OH($v = 9$) + O using both limiting values of $k_{O2bO}$, the rate constant for removal of $O_2$ ($b$, $v = 0$) by O atoms.

Equations M10 to M15 used to calculate the contributions of the new source contain several kinetics parameters and variables, many of which have significant uncertainties. We will now consider the kinetics inputs before discussing specific details pertinent to the model atmospheric composition used. To estimate the uncertainty for the results presented in Fig. 2, we considered the uncertainty of all kinetic parameters in Eqs. M10 to M15 at a nominal temperature of 200 K. We used the information listed in Table 1 and an uncertainty estimate of 10% for the nascent yield $y_9$ based on the uncertainties reported for the experimental measurements of Klenerman and Smith (*46*). The largest uncertainty contributions arise from parameters $y_{O2b}$, LT($OH_9$), and $k_{OH9NM}$ with uncertainties of 25, 23, and 22%, respectively. The combined uncertainty of all parameters propagated through the formulas for $O_2$ AB generated from OH($v = 9$) + O amounts to an SD of 57%.

As already mentioned, the [$N_2$], [$O_2$], [H], and temperature inputs are the profiles of the NRLMSISE-00 model for the time of the rocket launch of interest. The atomic hydrogen layer displays a steep "ledge" near 80 km where its number density increases by almost an order of magnitude within a few kilometers. Moreover, the layer and its peak near 85 km may move during the night in a manner not accurately captured by the NRLMSISE-00 model (*30*). Thus, the total intensity of the new source for $O_2$ AB could be affected, especially the slope of the emission's onset at altitudes below 85 km.

The intensity of the OH($v$) + O source of $O_2$ AB strongly depends on atomic oxygen. Accurate determination of the O-atom profile has been a long-standing challenge for upper atmospheric studies, and simultaneous measurements of O atoms are usually missing from nightglow observations. Such information is available for the ETON and NLTE sounding rocket campaigns. Nevertheless, a discussion of substantial issues with these measurements is warranted. For ETON, Greer *et al.* (*40*) summarized the difficulties with partial detector saturation and signal interference in the measurements and how these were handled. The atomic oxygen input for our calculations is from the ETON P232H payload, the first of two payloads that performed these measurements. For the ETON $O_2$ AB dataset, we used the average of two measurements from payloads P230H and P227H, launched 21 and 22 min before and after P232H (O-atom profile), respectively. The atomic oxygen profile from payload P232H can be considered representative of the conditions during the two $O_2$ AB measurements that preceded and followed it. Nevertheless, the second ETON O-atom profile (P234H), recorded approximately 126 min after the first (P232H), differed significantly at most altitudes and had a peak O-atom concentration that was larger than that of P232H by approximately 35%. Thus, while the choice of the datasets aims at mitigating any inconsistencies in the measurements, we cannot exclude the possibility of systematic errors.

The NLTE data have its own set of challenges, mainly related to the calibration of the resonance fluorescence measurements. The O-atom dataset from the descent of the NLTE-2 flight was calibrated according to the work of Hedin *et al.* (*32*). These authors proposed a method that uses nightglow intensity profiles ($O_2$ Chamberlain and AB bands) and the available empirical equations that relate the observed intensity to the O-atom concentration. From a study of several measured O-atom profiles, Hedin *et al.* (*32*) found that calibrating them in this manner resulted in an improvement of more than one order of magnitude in the spread of the retrieved O-atom concentrations. Using this approach for the NLTE-2 descent, we find an O-atom concentration peak of $4.2 \times 10^{11}$ atoms/$cm^3$ (Fig. 2). For the NLTE-2 ascent, Hedin *et al.* (*32*) obtained values from $4.4 \times 10^{11}$ to $4.7 \times 10^{11}$ atoms/$cm^3$. The ascent and descent flight trajectories are separated by several kilometers and are likely subjected to different aerodynamic conditions. Given the uncertainties in the measurements and their calibration, and the fact that we

now know that multiple production mechanisms are active, significant systematic errors cannot be excluded. Several authors have also considered complications in similar nightglow measurements such as the possibility of transient rocket-induced glow, nonlinearities in the measurements, or other contaminating emissions (*32*, *47*, *48*). The availability of accurate information on the atomic oxygen layer remains a challenge for the analysis and interpretation of nightglow emissions. Nevertheless, the uncertainties in the ETON and NLTE-2 atomic oxygen profiles do not put in question the conclusion that OH($v$ = 9) + O multiquantum relaxation is a significant source of $O_2$ AB emission.

### Consistency check for OH($v$ = 9) density

We can examine whether the OH($v$ = 9) number density implied by the calculations of the OH($v$ = 9) + O $O_2$ AB emission source is realistic. Some relevant information is available because ETON payload P228H obtained the emission profile of the (8,3) OH Meinel band (*49*). Figure S1 presents the OH($v$ = 8) concentration as a function of altitude, inferred from the P228H (8,3) OH Meinel band emission measurement using an Einstein coefficient of 0.9336 $s^{-1}$, reported by Xu *et al.* (*22*). The figure also presents the calculated [OH($v$ = 9)] using Eq. M10. For this calculation, the second O-atom measurement (P234H) was used as input because it is the closest one in time—the (8,3) OH band emission was measured ~26 min before P234H and 100 min after P232H (first O-atom measurement). The integrated OH($v$ = 8) population corresponding to the ETON observation is approximately 50% larger than that calculated for OH($v$ = 9), in very good agreement with observations of the OH(8)/OH(9) ratio for the Meinel band emission reported in the literature (*12*, *14*, *50*).

### O + O + M association and the new source for $O_2$ AB emission

Having established the important role of the source for $O_2$ AB emission from OH($v$ = 9) + O multiquantum relaxation, it is informative to consider the three-body O + O + M association reaction and the implications of the new findings. The generally accepted mechanism for the formation of $O_2$ AB emission from O-atom association was established in the 1980s (*15*, *17*, *18*). As mentioned, it involves excitation energy transfer from an initially formed electronically excited precursor to $O_2(b, v = 0)$. The exact nature of the excited precursor(s) and the detailed mechanistic steps are not well understood. This mechanism can be summarized by reactions M16 to M19

$$O + O + M \rightarrow O_2^* + M \; (M = O_2, N_2, O) \quad \text{(M16)}$$

$$O_2^* + O_2 \rightarrow O_2(b, v = 0) + O_2 \quad \text{(M17)}$$

$$O_2(b, v = 0) + M \; (M = O_2, N_2, O) \rightarrow \text{products} \quad \text{(M18)}$$

$$O_2(b, v = 0) \rightarrow O_2(X) + h\nu \quad \text{(M19)}$$

Assuming steady-state conditions, the concentration of $O_2(b, v = 0)$ is given by (*15*)

$$[O_{2b0}] = y_p \times k_{OOM} \times [O]^2 \times [M] \times y_{pO2} \times k_{pO2} \times [O_2] / \{LT(O_{2b0}) \times LT(O_2^*)\} \quad \text{(M20)}$$

The parameters $k_{OOM}$, $k_{pO2}$, $y_p$, and $y_{pO2}$ represent the rate constants and yields for processes M16 and M17, respectively. The term $LT(O_2^*)$ describes the loss rate of the electronically excited precursor

$$LT(O_2^*) = A_{O2^*} + k_{pO} \times [O] + k_{pO2} \times [O_2] + k_{pN2} \times [N_2] \quad \text{(M21)}$$

Equations M20 and M11 have a rather similar dependence on [O], [$O_2$], and [M]. This explains, in part, why the empirical equations for the $O_2$ AB emission available in the literature since the 1980s were found to describe reasonably well the observed altitude dependence of the emission and have been used to assess this emission and retrieve atomic oxygen profiles (*17*, *18*, *32*). Nevertheless, it is important to reiterate the fact that the nature of the $O_2$* precursor and the relevant mechanistic pathways originating from O + O + M are not well known. Moreover, the rate constants and yields $k_{pi}$ and $y_{pi}$ have not been quantified at mesospheric temperatures. In the literature, the parameters of the relevant empirical equations were simply adjusted to account for the observed $O_2$ AB emission intensity.

From Fig. 2, it is evident that the contribution of the source of $O_2$ AB emission from the OH($v$ = 9) + O process M5 peaks at a slightly lower altitude than the observed profile. The remainder emission originates from additional contributions by OH($v$ = 5 to 8) + O and termolecular association O + O + M. The former can be expected to have a rather similar altitude dependence to that of OH($v$ = 9) + O. Therefore, given the presence of the OH($v$) + O new source of $O_2$ AB emission, the reaction mechanisms M16 to M19 provide a less than adequate description of the O + O + M contributions to the $O_2$ AB emission, which peak at a higher altitude than those from OH($v$ = 9) + O. This is a telltale sign that contributions to the $O_2$ AB emission from O + O + M beyond the previously accepted basic mechanism most likely involve additional interactions with O atoms. The mechanism summarized in reactions M16 to M19 appears to be an oversimplification. Numerous relaxation pathways can lead from the multitude of electronically excited $O_2$ states near the dissociation limit to the $O_2(b, v)$ vibrational level manifold and eventually to $O_2(b, v = 0)$ (*16*). Oxygen atoms undoubtedly play a significant role in these processes. As already mentioned, laboratory experiments determined that the rate constants for vibrational relaxation of $O_2(b, v = 1)$ by O and $O_2$ are comparable at room temperature (*19*, *20*). The faster the relaxation of $O_2(b, v > 1)$ levels by O atoms occurs compared with the relaxation of $O_2(b, v = 1)$ by O, the larger the influence O atoms will have in the population flow through the $O_2(b)$ vibrational level manifold toward $O_2(b, v = 0)$. Although not directly relevant to $O_2(b, v)$ + O, we note that the removal of OH($v$ = 9) by O atoms at 298 K is faster than that of OH($v$ = 1) by one order of magnitude (*21*, *51*). It follows that we could include one more process in the mechanism for O + O + M generation of $O_2$ AB emission

$$O_2^* + O \rightarrow O_2(b, v = 0) + O \quad \text{(M22)}$$

The revised Eq. M20 for the steady-state concentration of $O_2(b, v = 0)$ when process M22 is included can be written as in reference (*15*)

$$[O_{2b0}] = y_p \times k_{OOM} \times [O]^2 \times [M] \times \{y_{pO2} \times k_{pO2} \times [O_2] + y_{pO} \times k_{pO} \times [O]\} / \{LT(O_{2b0}) \times LT(O_2^*)\} \quad \text{(M23)}$$

Figure 3 presents the ETON and NLTE-2 data together with best-fit curves using Eq. M23 and the kinetics parameters of table S1. The room

temperature value of $k_{O2bO}$, $8 \times 10^{-14}$ cm$^3$ s$^{-1}$, was used in the calculations. The figure shows two limiting cases for the new source of the $O_2$ AB emission. First, we considered only OH($v$ = 9) + O as a lower limit for the source of $O_2$ AB. Then, for an upper limit, we assumed that OH($v$ = 5 to 8) produced from the H + $O_3$ reaction behave similarly to OH($v$ = 9) in collisions with O atoms. The corresponding yields for processes M17 and M23, ($y_{pO2}$, $y_{pO}$), in Fig. 3 (A to D) have the values (0.24, 0.11), (0.02, 0.16), (0.02, 0.41), and (0, 0.30), respectively. As expected, when a maximum contribution for OH($v$) + O is considered (Fig. 3, B and D), $y_{pO2}$ becomes less important than $y_{pO}$. The fact that the optimized values for each limiting case differ significantly between ETON and NLTE-2 (Fig. 3, A versus C, and B versus D) appears to indicate some inconsistencies in the description of the mechanism. Nevertheless, invoking process M22 improves the agreement with the observed profile and may be a first step toward a more complete description of the $O_2$ AB emission. Better characterization is still required of the mechanistic details of O + O + M association as well as the contributions from OH($v$ = 5 to 8) + O.

On the basis of the observed OH($v$) vibrational population distributions reported in the literature (*12*, *14*, *50*), the steady-state population of OH($v$ = 9) is approximately one order of magnitude less than the cumulative population in levels $v$ = 5 to 8 (Fig. 1C). This observation suggests that most of the observed $O_2$ AB emission below 95 km originates from OH($v$) + O. We eagerly envision that future studies will fully quantify the $O_2$ AB source from OH($v \geq 5$) + O and the elusive mechanism of O + O + M association.

## SUPPLEMENTARY MATERIALS

Supplementary material for this article is available at http://advances.sciencemag.org/cgi/content/full/5/3/eaau9255/DC1

Fig. S1. Relevant information on the OH Meinel band emission from the ETON rocket P228H.
Table S1. Processes and relevant kinetics parameters relevant to the generation of $O_2$ AB emission from O + O + M association.
Data S1. Data inputs and calculation outputs presented in the main text and Methods.
References (*52*, *53*)

## REFERENCES AND NOTES


1. J. W. Chamberlain, "The Airglow Spectrum" in *Physics of the Aurora and Airglow* (reprint of 1961 edition by American Geophysical Union, 1995), pp. 345–392.
2. J. A. Ångström, Spectrum des Nordlichts. *Ann. Phys.* **137**, 161–163 (1868).
3. L. Yntema, On the brightness of the sky and total amount of starlight. *Publ. Ast. Groningen* **22**, 1–55 (1909).
4. Lord Rayleigh, IV (R. J. Strutt), The light of the night sky: Its intensity variations when analysed by colour filters. *Proc. Roy. Soc. A* **106**, 117–137 (1924).
5. A. B. Meinel, The near-infrared spectrum of the night sky and aurora. *Publ. Astron. Soc. Pac.* **60**, 373–378 (1948).
6. J. Kaplan, Active oxygen. *Nature* **159**, 673 (1947).
7. G. Herzberg, The atmospheres of the planets. *J. R. Astron. Soc. Can.* **45**, 100–123 (1951).
8. D. R. Bates, M. Nicolet, The photochemistry of atmospheric water vapor. *J. Geophys. Res.* **55**, 301–327 (1950).
9. A. B. Meinel, OH emission bands in the spectrum of the night sky I. *Astrophys. J.* **111**, 555–564 (1950).
10. A. B. Meinel, OH emission bands in the spectrum of the night sky II. *Astrophys. J.* **112**, 120–130 (1950).
11. P. E. Charters, R. G. Macdonald, J. C. Polanyi, Formation of vibrationally excited OH by the reaction H + $O_3$. *Appl. Opt.* **10**, 1747–1754 (1971).
12. S. Adler-Golden, Kinetic parameters for OH nightglow modeling consistent with recent laboratory measurements. *J. Geophys. Res.* **102**, 19969–19976 (1997).
13. D. J. Baker, A. T. Stair Jr., Rocket measurements of the altitude distributions of the hydroxyl airglow. *Phys. Scr.* **37**, 611–622 (1998).
14. P. C. Cosby, T. G. Slanger, OH spectroscopy and chemistry investigated with astronomical sky spectra. *Can. J. Phys.* **85**, 77–99 (2007).
15. V. A. Krasnopolsky, Excitation of the oxygen nightglow on the terrestrial planets. *Planet. Space Sci.* **59**, 754–766 (2011).
16. T. G. Slanger, R. A. Copeland, Energetic oxygen in the upper atmosphere and the laboratory. *Chem. Rev.* **103**, 4731–4765 (2003).
17. I. C. McDade, D. P. Murtagh, R. G. H. Greer, P. H. Dickinson, G. Witt, J. Stegman, E. J. Llewellyn, L. Thomas, D. B. Jenkins, ETON 2: Quenching parameters for the proposed precursors of $O_2(b^1\Sigma_g^+)$ and $O(^1S)$ in the terrestrial nightglow. *Planet. Space Sci.* **34**, 789–800 (1986).
18. D. P. Murtagh, G. Witt, J. Stegman, I. C. McDade, E. J. Llewellyn, F. Harris, R. G. H. Greer, An assessment of proposed $O(^1S)$ and $O_2(b^1\Sigma_g^+)$ nightglow excitation parameters. *Planet. Space Sci.* **38**, 43–53 (1990).
19. D. A. Pejaković, R. A. Copeland, T. G. Slanger, K. S. Kalogerakis, Collisional removal of $O_2(b^1\Sigma_g^+, v = 1)$ by $O(^3P)$ atoms. *Chem. Phys. Lett.* **403**, 372–377 (2005).
20. D. A. Pejaković, E. R. Wouters, K. E. Phillips, T. G. Slanger, R. A. Copeland, K. S. Kalogerakis, Collisional removal of $O_2(b^1\Sigma_g^+, v = 1)$ by $O_2$ at thermospheric temperatures. *J. Geophys. Res.* **110**, A03308 (2005).
21. K. S. Kalogerakis, G. P. Smith, R. A. Copeland, Collisional removal of OH($X\ ^2\Pi, v = 9$) by O, $O_2$, $O_3$, $N_2$, and $CO_2$. *J. Geophys. Res.* **116**, D20307 (2011).
22. J. Xu, H. Gao, A. K. Smith, Y. Zhu, Using TIMED/SABER nightglow observations to investigate hydroxyl emission mechanisms in the mesopause region. *J. Geophys. Res. Atmos.* **117**, D0231 (2012).
23. M. G. Mlynczak, L. A. Hunt, J. C. Mast, B. Thomas Marshall, J. M. Russell III, A. K. Smith, D. E. Siskind, J.-H. Yee, C. J. Mertens, F. Javier Martin-Torres, R. Earl Thompson, D. P. Drob, L. L. Gordley, Atomic oxygen in the mesosphere and lower thermosphere derived from SABER: Algorithm theoretical basis and measurement uncertainty. *J. Geophys. Res. Atmos.* **118**, 5724–5735 (2013).
24. M. G. Mlynczak, L. A. Hunt, J. M. Russell III, B. Thomas Marshall, Updated SABER night atomic oxygen and implications for SABER ozone and atomic hydrogen. *Geophys. Res. Letters* **45**, 5735–5741 (2018).
25. K. S. Kalogerakis, D. Matsiev, R. D. Sharma, P. P. Wintersteiner, Resolving the mesospheric nighttime 4.3 μm emission puzzle: Laboratory demonstration of new mechanism for OH(v) relaxation. *Geophys. Res. Lett.* **43**, 8835–8843 (2016).
26. R. D. Sharma, P. P. Wintersteiner, K. S. Kalogerakis, A new mechanism for OH vibrational relaxation leading to enhanced $CO_2$ emissions in the nocturnal atmosphere. *Geophys. Res. Lett.* **42**, 4639–4647, (2015).
27. P. A. Panka, A. A. Kutepov, K. S. Kalogerakis, D. Janches, J. M. Russell, L. Rezac, A. G. Feofilov, M. G. Mlynczak, E. Yiğit, Resolving the mesospheric nighttime 4.3 μm emission puzzle: New model calculations improve agreement with SABER observations. *Atmos. Chem. Phys.* **17**, 9751–9760 (2017).
28. D. A. Pejaković, R. A. Copeland, T. G. Slanger, K. S. Kalogerakis, $O_2(b^1\Sigma_g^+, v = 0, 1)$ relative yields in $O(^1D)$ + $O_2$ energy transfer. *J. Chem. Phys.* **141**, 024303 (2014).
29. T. G. Slanger, D. A. Pejaković, O. Kostko, D. Matsiev, K. S. Kalogerakis, Atmospheric dayglow diagnostics involving the $O_2$(b-X) Atmospheric band emission: Global Oxygen and Temperature (GOAT) mapping. *J. Geophys. Res. Space Phys.* **122**, 3640–3649 (2017).
30. J. M. Picone, A. E. Hedin, D. P. Drob, A. C. Aikin, NRLMSISE-00 empirical model of the atmosphere: Statistical comparisons and scientific issues. *J. Geophys. Res. Space Phys.* **107**, 1468 (2002).
31. J. Burkholder, J. Abbatt, R. Huie, C. Kolb, V. Orkin, P. Wine, S. Sander, J. Barker, M. Kurylo, D. M. Wilmouth, Chemical kinetics and photochemical data for use in atmospheric studies: Evaluation Number 18, JPL Publication 15-10, Jet Propulsion Laboratory, California Institute of Technology, Pasadena, CA (2015).
32. J. Hedin, J. Gumbel, J. Stegman, G. Witt, Use of $O_2$ airglow for calibrating direct atomic oxygen measurements from sounding rockets. *Atmos. Meas. Tech.* **2**, 801–812 (2009).
33. P. A. Panka, A. A. Kutepov, L. Rezac, K. S. Kalogerakis, A. G. Feofilov, D. Marsh, D. Janches, E. Yiğit, Atomic oxygen retrieved from the SABER 2.0 and 1.6 μm radiances using new first-principles nighttime OH(v) model. *Geophys. Res. Lett.* **45**, 5798–5803 (2018).
34. K. S. Kalogerakis, T. G. Slanger, E. A. Kendall, T. R. Pedersen, M. J. Kosch, B. Gustavsson, M. T. Rietveld, Remote oxygen sensing by ionospheric excitation (ROSIE). *Ann. Geophys.* **27**, 2183–2189 (2009).
35. M. Allen, Y. L. Yung, J. W. Waters, Vertical transport and photochemistry in the terrestrial mesosphere and lower thermosphere (50–120 km). *J. Geophys. Res. Space Phys.* **86**, 3617–3627 (1981).
36. M. Allen, J. I. Lunine, Y. L. Yung, The vertical distribution of ozone in the mesosphere and lower thermosphere. *J. Geophys. Res. Atmos.* **89**, 4841–4872 (1984).
37. M. V. Belikovich, M. Yu. Kulikov, M. Grygalashvyly, G. R. Sonnemann, T. S. Ermakova, A. M. Feigin, Ozone chemical equilibrium in the extended mesopause under the nighttime conditions. *Adv. Space Res.* **61**, 426–432 (2018).
38. J. S. A. Brooke, P. F. Bernath, C. M. Western, C. Sneden, M. Afşar, G. Li, I. E. Gordon, Line strengths of rovibrational and rotational transitions in the $X^2\Pi$ ground state of OH. *J. Quant. Spectrosc. Radiat. Transf.* **168**, 142–157 (2016).

39. B. D. Sharpee, T. G. Slanger, O($^1D_2$-$^3P_{2,1,0}$) 630.0, 636.4, and 639.2 nm forbidden emission line intensity ratios measured in the terrestrial nightglow. *J. Phys. Chem. A* **100**, 6707–6710 (2006).
40. R. G. H. Greer, D. P. Murtagh, I. C. McDade, P. H. G. Dickinson, L. Thomas, D. B. Jenkins, J. Stegman, E. J. Llewellyn, G. Witt, D. J. Mackinnon, E. R. Williams, ETON 1: A data base pertinent to the energy transfer in the oxygen nightglow. *Planet. Space Sci.* **34**(9), 771–788 (1986).
41. F.-J. Lübken, M. Rapp, J. Siebert, K.-H. Fricke, The thermal and dynamical state of the upper atmosphere during the first flight of the NLTE campaign, in *Proceedings of the 14th ESA/PAC Symposium on European Rocket and Balloon Programmes* and related research (ESA SP-437, 363–368), Potsdam, Germany 31 May to 3 June 1999.
42. Y. Liu, J. Peng, K. Reppert, S. Callahan, G. P. Smith, Laser measurements of the H atom + ozone rate constant at mesospheric temperatures. *J. Phys. Chem. A* **120**, 3855–3860 (2016).
43. J. I. Steinfeld, S. M. Adler-Golden, J. W. Gallagher, Critical survey on data on the spectroscopy and kinetics of ozone in the mesosphere and thermosphere. *J. Phys. Chem. Ref. Data* **16**, 911–951 (1987).
44. J. E. Thiebaud, R. A. Copeland, K. S. Kalogerakis, Vibrational relaxation of OH(v = 7) with O, $O_2$ and H, Abstract #SA43A-1752, American Geophysical Union Fall Meeting, San Francisco, California (2010).
45. T. G. Slanger, G. Black, Interactions of $O_2(b^1\Sigma_g^+)$ with O($^3P$) and $O_3$. *J. Chem. Phys.* **70**, 3434–3438 (1979).
46. D. Klenerman, I. W. M. Smith, Infrared chemiluminescence studies using a SISAM spectrometer. Reactions producing vibrationally excited OH. *J. Chem. Soc. Faraday Trans. 2* **83**, 229–241 (1987).
47. R. J. Thomas, Analysis of atomic oxygen, the green line, and Herzberg bands in the lower thermosphere. *J. Geophys. Res. Space Phys.* **86**, 206–210 (1981).
48. D. E. Siskind, W. E. Sharp, A comparison of measurements of the oxygen nightglow and atomic oxygen in the lower thermosphere. *Planet. Space Sci.* **39**, 627–639 (1991).
49. I. C. McDade, E. J. Llewellyn, D. P. Murtagh, R. G. H. Greer, ETON 5: Simultaneous Rocket Measurements of OH Meinel $\Delta v = 2$ sequence and the (8,3) band emission profiles in the nightglow. *Planet. Space Sci.* **35**(9), 1137–1147 (1987).
50. A. Migliorini, J. C. Gérard, L. Soret, G. Piccioni, F. Capaccioni, G. Filacchione, M. Snels, F. Tosi, Terrestrial OH nightglow measurements during the Rosetta flyby. *Geophys. Res. Lett.* **42**, 5670–5677 (2015).
51. A. Khachatrian, P. J. Dagdigian, Vibrational relaxation of OH by oxygen atoms. *Chem. Phys. Lett.* **415**, 1–5 (2005).
52. G. P. Smith, R. Robertson, Temperature dependence of oxygen atom recombination in nitrogen after ozone photolysis. *Chem. Phys. Lett.* **458**, 6–10 (2008).
53. D. L. Huestis, "Current laboratory experiments for planetary aeronomy," in *Atmospheres in the Solar System: Comparative Aeronomy*, AGU Monogr, M. Mendillo, A. Nagy, J. H. Waite, Eds. (American Geophysical Union, 2002), vol. 130, pp. 245–258.


**Acknowledgments:** I thank R. N. Zare, K. Bergmann, and T. G. Slanger for continued support throughout my career; J. P. Simons and M. Brouard for introducing me to the subtleties of the hydroxyl radical; the members of SRI International's (SRI) Molecular Physics Laboratory (1956–2014) for mentoring and remarkable legacy in upper atmospheric science; W. C. Olson for outstanding laboratory technical support; J. Hedin for providing data from the NLTE-2 sounding rocket campaign; R. D. Sharma, P. P. Wintersteiner, A. A. Kutepov, and P. A. Panka for insightful discussions; and J. Graham, K. Vamvaca, D. Matsiev, P. C. Cosby, and T. G. Slanger for comments on the manuscript. **Funding:** The seeds for this work were planted by a series of laboratory experimental projects at SRI over the course of two decades supported by the Aeronomy Program of the U.S. National Science Foundation (NSF) and the Geospace Science Program of the U.S. NASA. The specific data analysis and other preparations pertaining to this manuscript were supported by NSF award AGS-1441896, NASA award 80NSSC17K0638, and SRI internal research and development funds.
**Author contributions:** The author conceived the ideas for this endeavor, performed the data analysis, and wrote the manuscript. **Competing interests:** The author declares that he has no competing interests. **Data and materials availability:** All data needed to evaluate the conclusions in the paper are present in the paper and/or the Supplementary Materials. Additional data related to this paper may be requested from the author.

Submitted 27 July 2018
Accepted 31 January 2019
Published 20 March 2019
10.1126/sciadv.aau9255

**Citation:** K. S. Kalogerakis, A previously unrecognized source of the $O_2$ Atmospheric band emission in Earth's nightglow. *Sci. Adv.* **5**, eaau9255 (2019).

Science Advances

# A previously unrecognized source of the $O_2$ Atmospheric band emission in Earth's nightglow

Konstantinos S. Kalogerakis

*Sci Adv* **5** (3), eaau9255.
DOI: 10.1126/sciadv.aau9255